Optically induced spin current in monolayer math xmlns="http://www.w3.org/1998/Math/MathML">msub>mi >NbSe/mi>mn>2/mn>/msub>/math>

Ren Habara and Katsunori Wakabayashi

Phys. Rev. B **103**, L161410 — Published 27 April 2021

DOI: 10.1103/PhysRevB.103.L161410

Optical induced Spin Current in Monolayer $NbSe_2$

Ren Habara[1] and Katsunori Wakabayashi[1,2,3]

[1]*Department of Nanotechnology for Sustainable Energy, School of Science and Technology, Kwansei Gakuin University, Gakuen 2-1, Sanda 669-1337, Japan*
[2]*National Institute for Materials Science (NIMS), Namiki 1-1, Tsukuba 305-0044, Japan*
[3]*Center for Spintronics Research Network (CSRN), Osaka University, Toyonaka 560-8531, Japan*

(Dated: April 21, 2021)

Monolayer $NbSe_2$ is a metallic two-dimensional (2D) transition-metal dichalcogenide material. Owing to the lattice structure and the strong atomic spin-orbit coupling (SOC) field, monolayer $NbSe_2$ possesses Ising-type SOC which acts as effective Zeeman field, leading to the unconventional topological spin properties. In this paper, we numerically calculate spin-dependent optical conductivity of monolayer $NbSe_2$ using Kubo formula based on an effective tight-binding model which includes d_{z^2}, $d_{x^2-y^2}$ and d_{xy} orbitals of Nb atom. Numerical calculation indicates that the up- and down-spin have opposite sign of Hall current, so the pure spin Hall current can be generated in monolayer $NbSe_2$ under light irradiation, owing to the topological nature of monolayer $NbSe_2$, i.e., finite spin Berry curvature. The spin Hall angle is also evaluated. The optical induced spin Hall current can be enhanced by the electron doping and persists even at room temperature. Our results will serve to design opt-spintronics devices such as *spin current harvesting by light irradiation* on the basis of 2D materials.

Transition-metal dichalcogenide (TMDC) is a new class of two-dimensional (2D) electronic systems and provides a platform to design new functional opt-electronic devices.[1–5] In TMDC, electronic properties crucially depend on the combination of metal and chalcogen atoms.[6,7] Because of weak van der Waals forces between layers, monolayer of TMDC can be easily exfoliated and exhibit many fascinating properties such as valley-dependent optical selection rule[8–11] and spin Hall effect (SHE).[12–15] In particular, monolayer $NbSe_2$ belongs to monolayer of group-V TMDC MX_2 (M=Nb, Ta; X=S, Se), and is known to show metallic behavior with superconducting phase transition at low temperature.[16–19] Monolayer $NbSe_2$ has a hexagonal lattice structure but with no spatial inversion symmetry and possesses out-of-plane mirror symmetry. Owing to the lattice structure and strong atomic spin-orbit coupling (SOC) field, monolayer $NbSe_2$ possesses Ising-type SOC,[17–23] i.e., effective Zeeman field that locks electron spin to out-of-plane directions by in-plane momentum and provides the unconventional topological spin properties.

In this paper, we show that pure spin Hall current can be generated in monolayer $NbSe_2$ by light irradiation, owing to the topological nature of monolayer $NbSe_2$, i.e., finite spin Berry curvature. Figures 1 (a) and (b) show the top and side views of monolayer $NbSe_2$, respectively, where a layer of Nb atoms is sandwiched by two layers of Se atoms. From top view, monolayer $NbSe_2$ has a hexagonal lattice structure but with no spatial inversion symmetry. Also, from the side view, it respects out-of-plane mirror symmetry. Figure 1 (c) shows the corresponding first Brillouin Zone (BZ). We employ a multi-orbitals tight-binding model (TBM) which includes d_{z^2}, $d_{x^2-y^2}$ and d_{xy} orbitals of Nb atom to describe the electronic states of $NbSe_2$.[17,24] The eigenvalue equation for TBM is $\hat{H}(\boldsymbol{k})|u_{n\boldsymbol{k}}\rangle = E_{n\boldsymbol{k}}|u_{n\boldsymbol{k}}\rangle$, where $\boldsymbol{k} = (k_x, k_y)$ is the wavenumber vector, $E_{n\boldsymbol{k}}$ is the eigenvalue and $n = 1, 2, \cdots, 6$ is the band index. The eigenvector is defined as $|u_{n\boldsymbol{k}}\rangle = \left(c_{n\boldsymbol{k},d_{z^2},\uparrow}, c_{n\boldsymbol{k},d_{xy},\uparrow}, c_{n\boldsymbol{k},d_{x^2-y^2},\uparrow}, c_{n\boldsymbol{k},d_{z^2},\downarrow}, c_{n\boldsymbol{k},d_{xy},\downarrow}, c_{n\boldsymbol{k},d_{x^2-y^2},\downarrow}\right)^T$, where $(\cdots)^T$ indicates the transpose of vector and $c_{n\boldsymbol{k}\tau s}$ means the amplitude at atomic orbital τ with spin s for the nth energy band at $\boldsymbol{k}$. The Hamiltonian with the SOC can be written as

$$\hat{H}(\boldsymbol{k}) = \hat{\sigma}_0 \otimes \hat{H}_{TNN}(\boldsymbol{k}) + \hat{\sigma}_z \otimes \frac{1}{2}\lambda_{SOC}\hat{L}_z \tag{1}$$

with

$$\hat{H}_{TNN}(\boldsymbol{k}) = \begin{pmatrix} V_0 & V_1 & V_2 \\ V_1^* & V_{11} & V_{12} \\ V_2^* & V_{12}^* & V_{22} \end{pmatrix} \tag{2}$$

and

$$\hat{L}_z = \begin{pmatrix} 0 & 0 & 0 \\ 0 & 0 & -2i \\ 0 & 2i & 0 \end{pmatrix}. \tag{3}$$

Here, $\hat{\sigma}_0$ and $\hat{\sigma}_z$ are Pauli matrices, and λ_{SOC} is the Ising-type SOC parameter. In monolayer $NbSe_2$, $\lambda_{SOC} = 0.0784$ eV. $\hat{H}_{TNN}(\boldsymbol{k})$ includes the electron hoppings only among three d-orbitals of Nb atoms, which are assumed up to third-nearest neighbor sites as shown in Fig. 1 (a). Here, green, red and blue arrows indicate hopping vectors $\boldsymbol{R_i}$ $(i = 1, 2, \cdots, 6)$ pointing to nearest-neighbor (n.n) sites, the vectors $\tilde{\boldsymbol{R}}_{\boldsymbol{j}}$ $(j = 1, 2, \cdots, 6)$ pointing to next n.n sites and the vectors $2\boldsymbol{R_i}$ pointing to third n.n sites, respectively. The details of matrix elements V_0, V_1, V_2, V_{11}, V_{12} and V_{22} can be found in Supplementary material.[25] Figure 1 (d) shows the energy band structure of monolayer $NbSe_2$ along the line passing through the high-symmetric points of 1st BZ and the corresponding density of states (DOS). Here, red and blue lines indicate spin-up and spin-down states. Monolayer $NbSe_2$ is metallic, but a large energy band gap between the partially filled valence bands and empty conduction bands. Also, the Ising-type SOC provides the opposite spin splitting at the valence band edges in K and K′ points, and time-reversal symmetry protection.

We numerically calculate spin-dependent optical conductivity of $NbSe_2$ using Kubo formula[26–35] based on an effective TBM, and find the photo-induced generation of pure spin

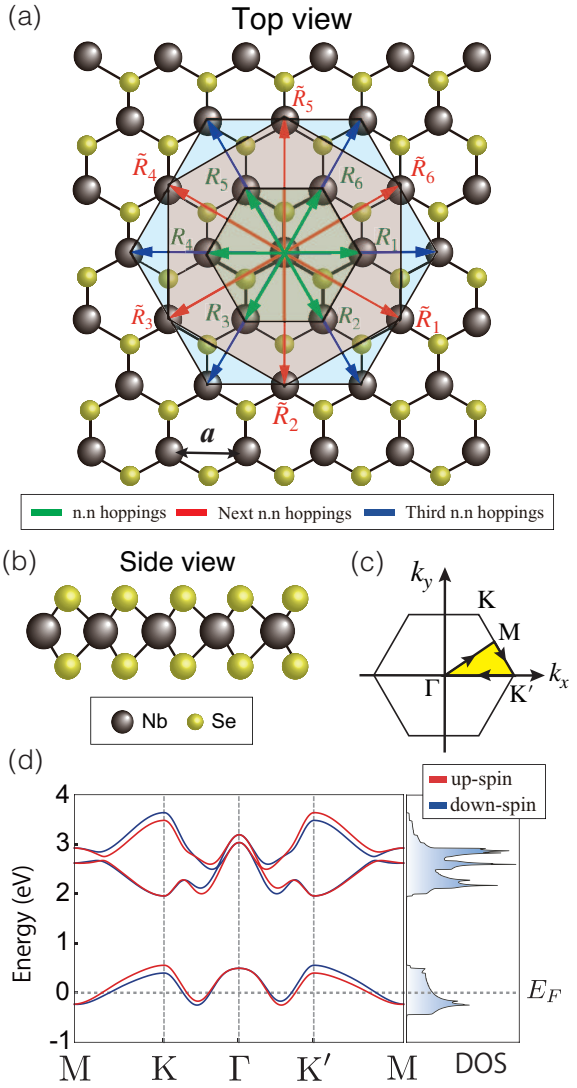

FIG. 1. Crystal structure of monolayer $NbSe_2$ which consists of Nb (black) and Se (yellow) atoms. (a) Top view and (b) side view of the lattice structure. Green, red and blue arrows indicate hopping vectors $\boldsymbol{R_i}$ $(i = 1, 2, \cdots, 6)$ pointing to n.n sites, the vectors $\tilde{\boldsymbol{R}}_{\boldsymbol{j}}$ $(j = 1, 2, \cdots, 6)$ pointing to next n.n sites and the vectors $2\boldsymbol{R_i}$ pointing to third n.n sites, respectively. a is the lattice constant. (c) 1st BZ of monolayer $NbSe_2$. (d) Energy band structure and DOS of $NbSe_2$ with SOC parameter $\lambda_{SOC} = 0.0784$ eV. Fermi level is set to zero.

Hall current.[36–38] The spin-dependent optical Hall conductivity can be given as

$$\sigma_{xy}^{spin}(\omega) = \frac{i\hbar e}{S}\sum_{\boldsymbol{k}}\sum_{nm}\frac{f(E_{n\boldsymbol{k}}) - f(E_{m\boldsymbol{k}})}{E_{m\boldsymbol{k}} - E_{n\boldsymbol{k}}} \cdot \frac{\langle u_{n\boldsymbol{k}}|\hat{j}_x^{spin}|u_{m\boldsymbol{k}}\rangle\langle u_{m\boldsymbol{k}}|\hat{v}_y|u_{n\boldsymbol{k}}\rangle}{E_{m\boldsymbol{k}} - E_{n\boldsymbol{k}} - \hbar\omega - i\eta}, \tag{4}$$

where $n(m)$ indicates the band index including spin degree of freedom, $|u_{n\boldsymbol{k}}\rangle$ is the eigen function with the eigen energy $E_{n\boldsymbol{k}}$ and $f(E_{n\boldsymbol{k}})$ is Fermi-Dirac distribution function. η is infinitesimally small real number, and S is the area of system. Also, $\hat{j}_x^{spin}$ is the spin current operator, and written as $\hat{j}_x^{spin} = \frac{1}{2}\{\frac{\hbar}{2}\hat{\sigma}_z \otimes \hat{I}_3, \hat{v}_x\}$, where $\hat{I}_3$ is the 3×3 identity matrix and $(\hat{v}_x, \hat{v}_y) = \frac{1}{\hbar}(\frac{\partial \hat{H}}{\partial x}, \frac{\partial \hat{H}}{\partial y})$ is the group velocity operator. We add the superscript *spin* for the spin-dependent optical Hall conductivity in order to distinguish its conductivity from ordinary optical Hall conductivity without SOC. When we consider $\sigma_{xy}^{spin}(\omega)$ for direct current (DC) limit ($\omega = 0$), zero-temperature ($T = 0$ K) and clean limit ($\eta = 0$ eV), Equation (14) becomes

$$\sigma_{xy}^{spin} = \frac{e}{S}\sum_{\boldsymbol{k}}\Omega^{spin}(\boldsymbol{k}) \tag{5}$$

with

$$\Omega^{spin}(\boldsymbol{k}) = \hbar\sum_n f(E_{n\boldsymbol{k}})\sum_{m\neq n}\frac{-2\mathrm{Im}\langle u_{n\boldsymbol{k}}|\hat{j}_x^{spin}|u_{m\boldsymbol{k}}\rangle\langle u_{m\boldsymbol{k}}|\hat{v}_y|u_{n\boldsymbol{k}}\rangle}{(E_{m\boldsymbol{k}} - E_{n\boldsymbol{k}})^2}. \tag{6}$$

Here, $\Omega^{spin}(\boldsymbol{k})$ is spin Berry curvature of Bloch state,[26,33,39–46] and drives an anomalous transverse velocity[47,48] written as

$$v_\perp = -\frac{e}{\hbar}\boldsymbol{E}\times\Omega^{spin}(\boldsymbol{k}) \tag{7}$$

under the presence of an electric field $\boldsymbol{E}$.

Figure 2 (a) shows the 2D contour plot of spin Berry curvature in 1st BZ. It clearly shows the six-fold symmetry. However, for each spin state, its symmetry around Γ point reduces to three-fold symmetry because the energy band of monolayer $NbSe_2$ has opposite spin splitting around K and K′ points [see Figs. S2 (a) and (b)].[25] In Fig. 2 (b), the spin Berry curvature is plotted along the path passing through high-symmetric points of 1st BZ. Owing to the Fermi-Dirac distribution function in Eq. (6), the spin Berry curvature is vanished at valleys. This is very contrast from semiconducting MX_2 such as MoS_2, where valley current is induced owing to the finite Berry curvature at the valleys. In monolayer $NbSe_2$, valley current can be induced by the electron doping [see Figs. S4 (a) and (b)].[25] As can be seen in Fig. 2 (b), the spin Berry curvature has sharp peaks with the same sign, because the energy differences between up and down spin states become very small at the Fermi energy as can be confirmed in Fig. 1 (d). Figure 2 (c) shows Fermi energy dependence of spin-dependent Hall conductivity for several different SOC parameters. Since spin Hall conductivity is the summation of the spin Berry curvature over the momentum in DC limit, and can be calculated by using Eq. (5). It is noted that the spin Hall conductivity is enhanced by electron-doping. Thus, finite Berry curvature manifests the intrinsic SHE[45–47], i.e., the generation of transverse spin current by the application of electric field.

Figure 3 (a) shows the numerically calculated angular frequency dependence of spin-dependent optical Hall conductivity for several different SOC parameters. It is clearly seen that the large peak around 3.0 eV, i.e., the generation of spin Hall current in $NbSe_2$ ($\lambda_{SOC} = 0.0784$ eV) by light irradiation. The cases for $\lambda_{SOC} = 0.0392$ and 0 eV are also plotted for the comparison. It should be noted that the optical charge Hall conductivity is identically zero for arbitrary energy, because the

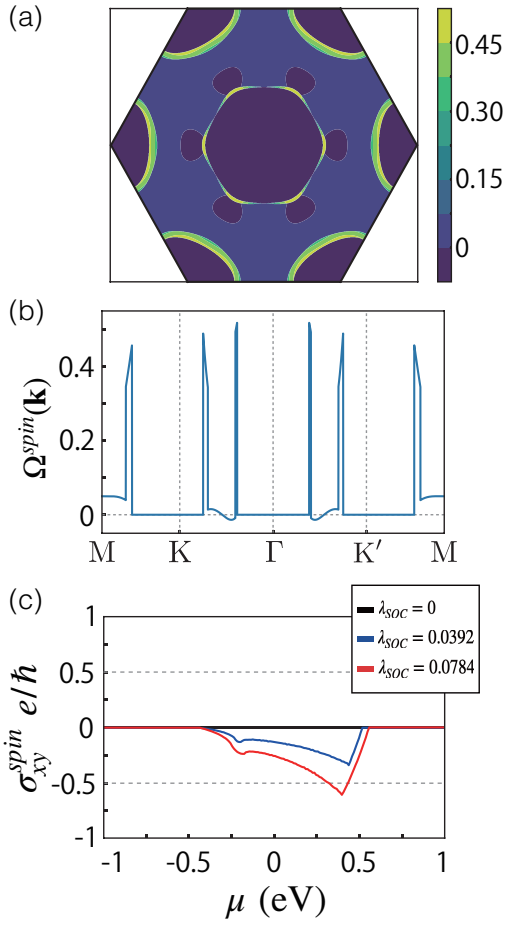

FIG. 2. Spin Berry curvature of monolayer $NbSe_2$ with SOC parameter $\lambda_{SOC} = 0.0784$ eV. (a) Contour plot in 1st BZ. (b) Plot along the path through the high-symmetric points in 1st BZ. (c) Fermi-level dependence of spin-dependent Hall conductivity σ_{xy}^{spin} of DC limit for several different SOC parameters. The unit of σ_{xy}^{spin} is $e^2/\hbar$.

charge Berry curvature has the anti-symmetric with the wave number, i.e., $\Omega^{charge}(\boldsymbol{k}) = -\Omega^{charge}(-\boldsymbol{k})$ [see Figs. S2 (c) and (d)].[25] Thus, the pure spin current can be induced by light irradiation in monolayer $NbSe_2$. Since the intensive peaks of σ_{xy}^{spin} appear in the range of $2.7-3.2$ eV, i.e., visible and ultraviolet range, monolayer $NbSe_2$ can be used for the application of *spin current harvesting by light irradiation*. The effect of optical induced spin Hall current is also robust to temperature, and is expected to be observed even in room temperature [see Fig. S5 (a)].[25]

Figure 3 (b) shows the angular frequency dependence of spin Hall angle (SHA),[26,36,46,49,50] which measures conversion efficiency from charge current to spin current. SHA is given as

$$\theta^{spin} = \frac{2e}{\hbar}\frac{\sigma_{xy}^{spin}}{\sigma_{xx}}, \tag{8}$$

where σ_{xx} is optical longitudinal conductivity[31,51,52] which is found in Fig. S5 (b).[25] SHA has divergence below about 2.1

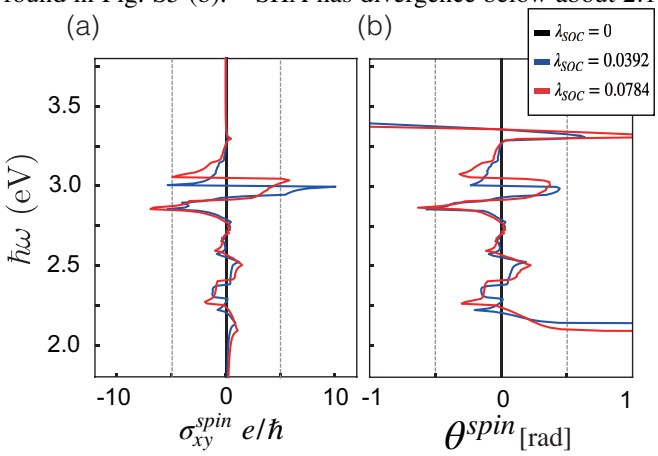

FIG. 3. Optical angular frequency dependence of (a) spin-dependent Hall conductivity $\sigma_{xy}^{spin}(\omega)$ of $E_F = 0$ eV and (b) SHA θ^{spin} for several different SOC parameters. The unit of $\sigma_{xy}^{spin}(\omega)$ is $e^2/\hbar$.

eV and above about 3.3 eV, because σ_{xx} becomes zero, where SHA becomes ill-defined. When the Hall conductivity has peak, the SHA also has larger value and then indicates that we can generate the pure spin current efficiently. Moreover, the observed optical induced pure Hall spin current is robust against the carrier doping. In particular, the pure spin current can be enhanced by electron-doping [see Fig. S6].[25] These results indicate that we can generate the spin Hall current efficiently by light irradiation using visible light of violet and enhance its magnitude by electron doping.

In conclusion, we have theoretically proposed that pure spin Hall current can be induced efficiently in monolayer $NbSe_2$ by irradiating the visible light. The origin of spin Hall current can be attributed by the finite spin Berry curvature owing to the Ising-type SOC in monolayer $NbSe_2$. It is also found that the optical induced spin Hall current can be enhanced by the electron doping and persists even in the room temperature[see Supplementary material].[25] Thus, monolayer $NbSe_2$ can be used for the source of pure spin current by using light irradiation. Our results will serve to design opt-spintronics devices such as *spin current harvesting by light irradiation* on the basis of 2D materials.

This work was supported by JSPS KAKENHI (Nos. JP21H01019, JP18H01154) and JST CREST (No. JPMJCR19T1).

[1] K. F. Mak, C. Lee, J. Hone, J. Shan, and T. F. Heinz, Phys. Rev. Lett. **105**, 136805 (2010).

[2] A. Splendiani, L. Sun, Y. Zhang, T. Li, J. Kim, C.-Y. Chim,

G. Galli, and F. Wang, Nano Lett. **10**, 1271 (2010).
[3] S. Tongay, J. Zhou, C. Ataca, K. Lo, T. S. Matthews, J. Li, J. C. Grossman, and J. Wu, Nano Lett. **12**, 5576 (2012).
[4] H. R. Gutiérrez, N. Perea-López, A. L. Elías, A. Berkdemir, B. Wang, R. Lv, F. López-Urías, V. H. Crespi, H. Terrones, and M. Terrones, Nano Lett. **13**, 3447 (2013).
[5] W. Zhao, Z. Ghorannevis, L. Chu, M. Toh, C. Kloc, P.-H. Tan, and G. Eda, ACS Nano **7**, 791 (2013).
[6] Q. H. Wang, K. Kalantar-Zadeh, A. Kis, J. N. Coleman, and M. S. Strano, Nat. Nanotechnol. **7**, 699 (2012).
[7] M. Chhowalla, H. S. Shin, G. Eda, L.-J. Li, K. P. Loh, and H. Zhang, Nat. Chem. **5**, 263 (2013).
[8] H. Zeng, J. Dai, W. Yao, D. Xiao, and X. Cui, Nat. Nanotechnol. **7**, 490 (2012).
[9] K. F. Mak, K. He, J. Shan, and T. F. Heinz, Nat. Nanotechnol. **7**, 494 (2012).
[10] T. Cao, G. Wang, W. Han, H. Ye, C. Zhu, J. Shi, Q. Niu, P. Tan, E. Wang, B. Liu, and J. Feng, Nat. Commun. **3**, 887 (2012).
[11] H. Yu, X. Cui, X. Xu, and W. Yao, Natl. Sci. Rev. **2**, 57 (2015).
[12] J. Sinova, S. O. Valenzuela, J. Wunderlich, C. H. Back, and T. Jungwirth, Rev. Mod. Phys. **87**, 1213 (2015).
[13] P. N. Hai, J. Magn. Soc. Jpn. **44**, 137 (2020).
[14] Y. K. Kato, R. C. Myers, A. C. Gossard, and D. D. Awschalom, Science **306**, 1910 (2004).
[15] J. Wunderlich, B. Kaestner, J. Sinova, and T. Jungwirth, Phys. Rev. Lett. **94**, 047204 (2005).
[16] S. Kim and Y.-W. Son, Phys. Rev. B **96**, 155439 (2017).
[17] W.-Y. He, B. T. Zhou, J. J. He, N. F. Q. Yuan, T. Zhang, and K. T. Law, Commun. Phys. **1**, 40 (2018).
[18] X. Xi, Z. Wang, W. Zhao, J.-H. Park, K. T. Law, H. Berger, L. Forró, J. Shan, and K. F. Mak, Nat. Phys. **12**, 139 (2016).
[19] E. Sohn, X. Xi, W.-Y. He, S. Jiang, Z. Wang, K. Kang, J.-H. Park, H. Berger, L. Forró, K. T. Law, J. Shan, and K. F. Mak, Nat. Mater. **17**, 504 (2018).
[20] J. M. Lu, O. Zheliuk, I. Leermakers, N. F. Q. Yuan, U. Zeitler, K. T. Law, and J. T. Ye, Science **350**, 1353 (2015).
[21] Y. Saito, Y. Nakamura, M. S. Bahramy, Y. Kohama, J. Ye, Y. Kasahara, Y. Nakagawa, M. Onga, M. Tokunaga, T. Nojima, Y. Yanase, and Y. Iwasa, Nat. Phys. **12**, 144 (2016).
[22] B. T. Zhou, N. F. Q. Yuan, H.-L. Jiang, and K. T. Law, Phys. Rev. B **93**, 180501(R) (2016).
[23] L. Bawden, S. P. Cooil, F. Mazzola, J. M. Riley, L. J. Collins-McIntyre, V. Sunko, K. W. B. Hunvik, M. Leandersson, C. M. Polley, T. Balasubramanian, T. K. Kim, M. Hoesch, J. W. Wells, G. Balakrishnan, M. S. Bahramy, and P. D. C. King, Nat. Commun. **7**, 11711 (2016).
[24] G.-B. Liu, W.-Y. Shan, Y. Yao, W. Yao, and D. Xiao, Phys. Rev. B **88**, 085433 (2013).
[25] See Supplemetary Material at [URL will be inserted by publisher] for details of matrix elements in an effective Hamiltonian. It is also presented the doping and temperature effects on optical spin Hall conductivity.
[26] J. Qiao, J. Zhou, Z. Yuan, and W. Zhao, Phys. Rev. B **98**, 214402 (2018).
[27] G. Y. Guo, Y. Yao, and Q. Niu, Phys. Rev. Lett. **94**, 226601 (2005).
[28] P. Sengupta, S. Rakheja, and E. Bellotti, arXiv:1512.06734 (2015).
[29] V. Vargiamidis, P. Vasilopoulos, and G.-Q. Hai, J. Phys. Condens. Matter **26**, 345303 (2014).
[30] T. Tanaka, H. Kontani, M. Naito, T. Naito, D. S. Hirashima, K. Yamada, and J. Inoue, Phys. Rev. B **77**, 165117 (2008).
[31] A. Ferreira, J. Viana-Gomes, Y. V. Bludov, V. Pereira, N. M. R. Peres, and A. H. Castro Neto, Phys. Rev. B **84**, 235410 (2011).
[32] T. Morimoto, Y. Hatsugai, and H. Aoki, Phys. Rev. Lett. **103**, 116803 (2009).
[33] Y. Yao, L. Kleinman, A. H. MacDonald, J. Sinova, T. Jungwirth, D.-s. Wang, E. Wang, and Q. Niu, Phys. Rev. Lett. **92**, 037204 (2004).
[34] Z. Li and J. P. Carbotte, Phys. Rev. B **86**, 205425 (2012).
[35] M. Akita, Y. Fujii, M. Maruyama, S. Okada, and K. Wakabayashi, Phys. Rev. B **101**, 085418 (2020).
[36] S. Y. Huang, D. Qu, T. C. Chuang, C. C. Chiang, W. Lin, and C. L. Chien, Appl. Phys. Lett. **117**, 190501 (2020).
[37] W. Lin and C. L. Chien, arXiv:1804.01392 (2018).
[38] W.-Y. Shan, J. Zhou, and D. Xiao, Phys. Rev. B **91**, 035402 (2015).
[39] J. Sławińska, F. T. Cerasoli, H. Wang, S. Postorino, A. Supka, S. Curtarolo, M. Fornari, and M. B. Nardelli, 2D Mater. **6**, 025012 (2019).
[40] Y. Yao and Z. Fang, Phys. Rev. Lett. **95**, 156601 (2005).
[41] H. Da, Q. Song, P. Dong, H. Ye, and X. Yan, J. Appl. Phys. **127**, 023903 (2020).
[42] M. Gradhand, D. V. Fedorov, F. Pientka, P. Zahn, I. Mertig, and B. L. Györffy, J. Phys. Condens. Matter **24**, 213202 (2012).
[43] G. Qu, K. Nakamura, and M. Hayashi, arXiv:1901.05651 (2019).
[44] J. Kim, K.-W. Kim, D. Shin, S.-H. Lee, J. Sinova, N. Park, and H. Jin, Nat. Commun. **10**, 3965 (2019).
[45] G. Y. Guo, S. Murakami, T.-W. Chen, and N. Nagaosa, Phys. Rev. Lett. **100**, 096401 (2008).
[46] J. Zhou, J. Qiao, A. Bournel, and W. Zhao, Phys. Rev. B **99**, 060408(R) (2019).
[47] W. Feng, Y. Yao, W. Zhu, J. Zhou, W. Yao, and D. Xiao, Phys. Rev. B **86**, 165108 (2012).
[48] D. Xiao, M.-C. Chang, and Q. Niu, Rev. Mod. Phys. **82**, 1959 (2010).
[49] Y. Wang, P. Deorani, X. Qiu, J. H. Kwon, and H. Yang, Appl. Phys. Lett. **105**, 152412 (2014).
[50] W. Zhang, W. Han, S.-H. Yang, Y. Sun, Y. Zhang, B. Yan, and S. S. P. Parkin, Sci. Adv. **2**, e1600759 (2016).
[51] R. Kubo, J. Phys. Soc. Japan **12**, 570 (1957).
[52] S. Saberi-Pouya, T. Vazifehshenas, T. Salavati-fard, M. Farmanbar, and F. M. Peeters, Phys. Rev. B **96**, 075411 (2017).